CHAPTER 3

SENSING OF ARSENIC, CESIUM ION, AND CATALYTIC ACTIVITY OF HYDROGEN PEROXIDE, AND REMOVAL OF CESIUM ION THROUGH SYNTHESIZED PRUSSIAN BLUE NANOPARTICLES

3.1 Design of PBNPs-Modified Electrochemical Electrodes

3.1.1 Fabrication of PB nanoparticle-modified screen-printed electrodes

Screen-printed electrodes (SPE) are three-electrode configurations were created using silver, graphite, and Ag/AgCl pastes, as illustrated in Figure 3.1A; graphite was used for the working and counter electrodes, and Ag/AgCl was used for the reference electrode. The working electrode track of the freshly prepared SPE was modified using a Nordson dispenser containing PBNP-2 printing ink and desiccated at 380 K for one hour.

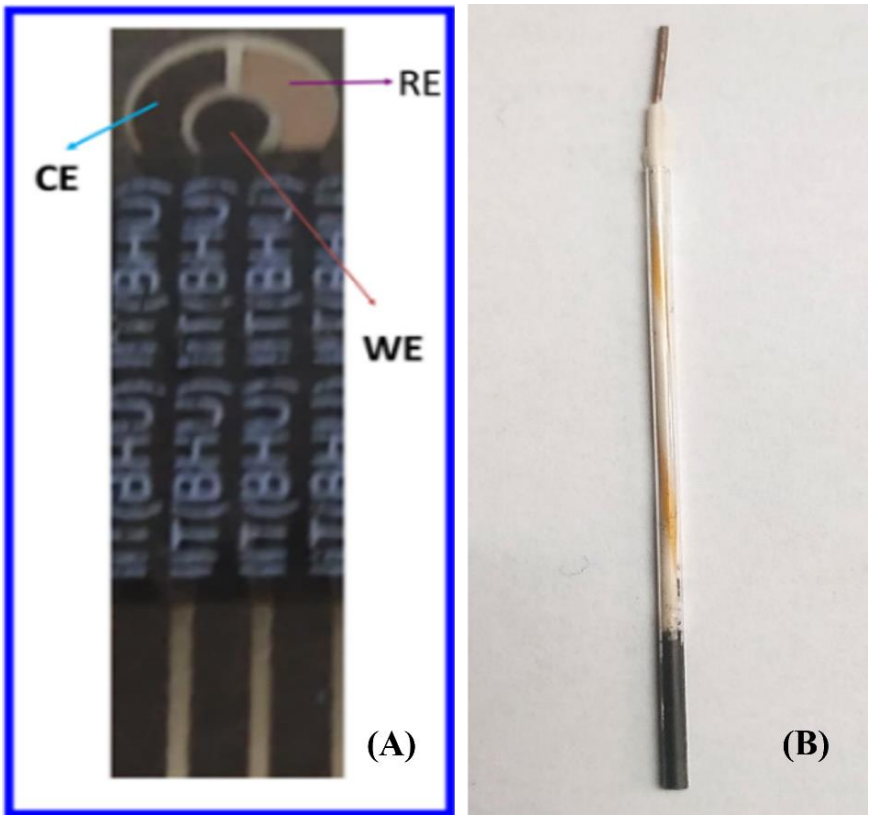

Figure 3.1. (A) Homemade screen-printed electrode (WE=working electrode, RE=Reference electrode, and CE=counter electrode), (B) PBNP-modified graphite paste electrode.

3.1.2 Fabrication of PBNPs-modified graphite paste electrode

The present study involved the preparation of active PBNP-1, PBNP-2, and PBNP-3 modified graphite paste through the amalgamation of PBNP-1/PBNP-2/PBNP-3, graphite powder, and nujol oil. The procedure for creating paste entails the combination of 5 µl of PBNP-1/PBNP-2/PBNP-3 with 9 mg graphite powder of spectroscopic grade, which is then subjected to sonication for 30 minutes. The resulting mixture is subsequently dried at 60 ^{0}C in a vacuum oven for the duration of an entire night. Graphite powder = 68% (w/w), PBNP adsorbed graphite = 2.5% (w/w), and nujol oil = 30% (w/w) were mixed to create an active PBNP-modified graphite paste. An active paste is put into a well in the electrode body that is 2 mm deep (Fig. 3.1B). The paste was meticulously smoothed onto a sheet of pristine butter paper.

3.2 Evaluation of PB Nanoparticle-Modified Electrodes

For PB nanoparticle-modified SPE, electrochemical studies like differential pulse voltammetry (DPV), cyclic voltammetry (CV), electrochemical impedance spectroscopy (EIS), and chronoamperometry were performed for AS(III), H2O2, and Cs ions. The study was conducted using a CHI Instruments Electrochemical Workstation Model 660 (Austin, TX, USA) with a working volume of 3 mL 0.1M KNO3 and a specially designed electrochemical cell that was equipped with an electrode holder. PB nanoparticle-modified electrodes were used as the working electrodes. The electrochemical cell was degassed through purging with nitrogen gas when necessary. For PBNP-modified graphite paste electrodes, electrochemical studies including CV, DPV, and EIS were performed in a three-electrode configuration.

3.2.1 Electrochemical Sensing through Screen-Printed Electrode

Recently, we demonstrated that PB nanoparticles served as an efficient nanomaterial for sensing and removal of As(III) (Pandey et.al. 2021). In order to understand the utility of PB for sensing and removal of cesium ions, it is important to discriminate the interaction of PB with hydrogen peroxide, arsenic (III), and cesium ions. Since PB nanoparticles are a well-known peroxidase mimetic, PB nanoparticle-modified screen-printed electrodes undergo a selective reduction of hydrogen peroxide close to 0.2 V vs. Ag/AgCl. Recent work (Pandey et.al. 2021) indicated that the variation in peak current as a function of hydrogen peroxide and arsenic (III) concentrations occurred in opposite directions, revealing the introduction of selective electrochemical sensing of these 2 analytes. Accordingly, there was an attempt to evaluate the electrochemical sensing of cesium ions under similar conditions was undertaken in order to understand the electrochemical behavior of the PB-modified electrode in the presence of these analytes.

3.2.1.1 Electrochemistry of PBNP-2 modified SPE in the Presence of As(III) and Hydrogen Peroxide

The electrochemistry of the PB nanoparticle-modified SPE in the presence of As(III) and H_2O_2 was examined using DPV (Figure 3.2), and EIS (Figure 3.3). In order to understand the dependence of DPV peak current on the analyte concentration, the variation in peak current was examined in the presence of H_2O_2. Since PB nanoparticles act as a potent peroxidase mimetic agent, enabling selective reduction of the same at the PB nanoparticle-modified electrode close to 0.2 V vs. Ag/AgCl. The results are shown in Figure 3.2A for change in peaks current in the absence and presence of hydrogen peroxide (0-10 mM). The

peak current increased with the concentration of hydrogen peroxide, indicating a direct relation between H_2O_2 and PB nanoparticle-mediated reduction resulting in a direct electrochemical transition of Fe^{2+}/Fe^{3+} couple. The increase in peak current was attributed to an increase in Fe^{3+} as a function of H_2O_2. Subsequently, we also examined the variation in the peak current of DPV under similar conditions as a function of the As(III) concentration as shown in Figure 3.2B. The following results were noted: (1) the peak current displayed a pH-dependent behavior, with relatively better variation in the peak current at a pH of 9.0 in the presence of As (III), and (2) the peak current tended to decrease with an increase in the concentration of As (III); the opposite trend was recorded in the presence of hydrogen per- oxide. An increase in Fe^{2+} as a function of As (III) concentration was recorded, suggesting the oxidation of As (III) into As (V). These findings clearly predict an analyte-dependent intervalence transition between Fe^{2+} and Fe^{3+}. To gain a better understanding of the electrochemical interface, we have further characterized the performance of the PB nanoparticle-modified electrode by electrochemical impedance spectroscopy.

The EIS of the PB nanoparticle-modified electrode is shown in Figure 3.3 in the absence and presence of various concentrations of H_2O_2 and As (III). The Nyquist plot in the absence and the presence of H_2O_2 and arsenite is shown in Figure 3.3A, B, respectively. The impedance spectra shown in Figure 3.3 include a semicircle portion, corresponding to charge transfer resistance, and a linear portion, corresponding to a diffusion-limited process. EIS of the bare PBNP-2 modified electrode (Figure 3.3) exhibited a nearly straight line; these features indicate the diffusion-limiting step of an electrochemical process. In addition, the electron-

transfer resistance (R_{et}) corresponds to the semicircle diameter. The semicircle diameter for the PBNP-2 modified electrode in the presence of H_2O_2 tended to decrease as compared to that of the PB nanoparticle-modified electrode in the presence of As (III) as shown in Figures 3.3A, B, respectively. This result indicates a predominantly diffusion-limiting step of the electrochemical process between PB nanoparticles and As (III) and electron-transfer resistance in the presence of H_2O_2; this result was associated with the analyte-dependent intervalence transition between Fe^{2+} and Fe^{3+}. The peak current of differential pulse voltammograms in the absence and the presence of As(III) and H_2O_2 was used to construct calibration plots for the electrochemical analysis of these analytes.

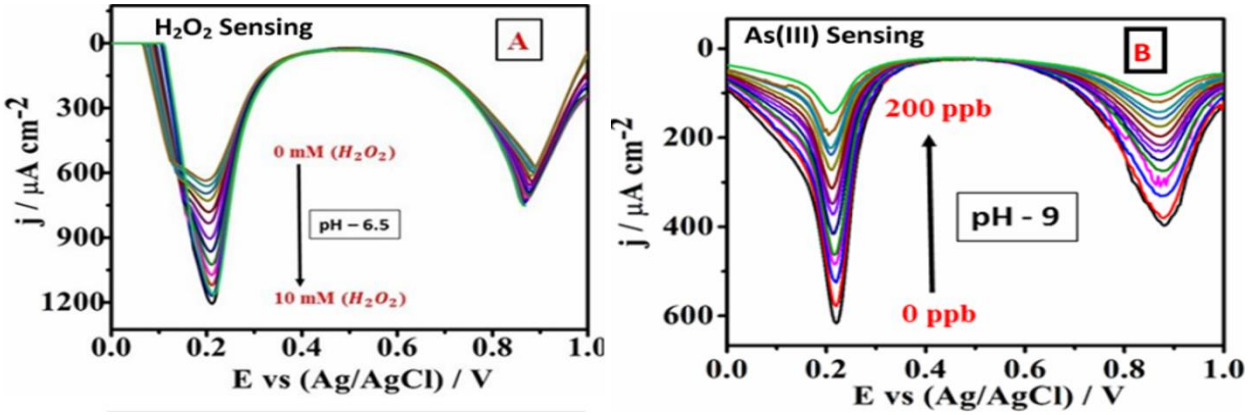

Figure 3.2. Differential pulse voltammetry of the PB nanoparticle-modified screen-printed electrode in the presence of varying concentrations of hydrogen peroxide. (A) (mM): 0.063, 0.126, 0.25, 0.4, 0.8, 1,2, 3, 4, 5, 8, 10, and As (III). (B) (ppb): 20, 40, 60, 80, 100, 120, 140, 160, 180, 200.

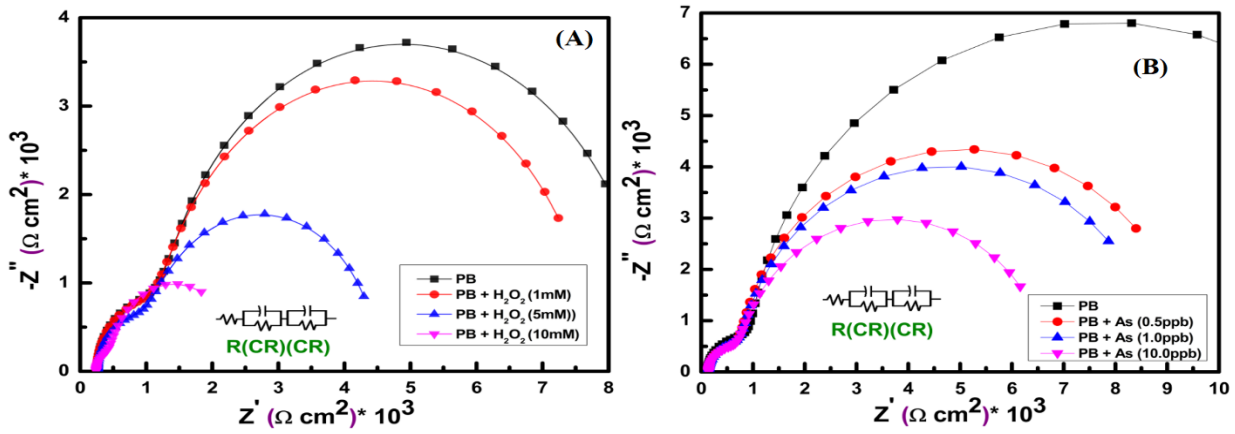

Figure 3.3 (A) Nyquist plot of the PB nanoparticle-modified electrode in the presence of varying concentrations of hydrogen peroxide, (B) Nyquist plot of the PB nanoparticle-modified electrode in the presence of varying concentrations of As (III).

The difference in peak current in the absence of the analyte (I_{pc}) and in the presence of the analyte (As (III)/H_2O_2) (I_{px}) was used to construct the calibration plot for the analysis of As (III) and H_2O_2 (e.g., [I_{px}-I_{pc}] vs. Log C, where C is the concentration of As (III) in ppm (Figure 3.4A) and H_2O_2 in mM (Figure 3.4B)). An excellent linear relationship with the lowest detection limit of 0.01 ppb of As (III) justified the use of the PB nanoparticle-mediated electrochemical approach of sensing of As (III); electrochemical oxidation of As (III) as well as the opposite reaction for hydrogen peroxide were demonstrated.

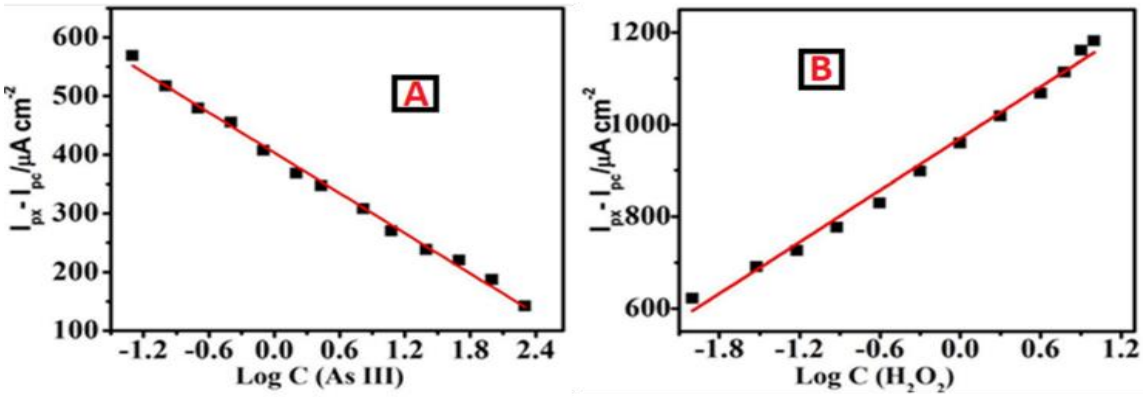

Figure 3.4. Calibration curve for the analysis of As(III) (A), and hydrogen peroxide (B) based on differential pulse voltammetry.

3.2.1.2 Electrochemistry of PBNP-2 modified SPE in the Presence of Cs ion

To understand the dependence of the electrochemical behavior of the PBNP-2 modified SPE as a function of the Cs concentration, we investigated the cyclic voltammogram of the same in the absence and in the presence of Cs ions (Figure 3.5). The results from the cyclic voltammograms as shown in Figure 3.5 revealed that the redox peak close to 0.22 V vs. Ag/AgCl did not change significantly, whereas the second redox couple of the PB nanoparticles close to 0.88 V vs. Ag/AgCl showed an increase in anodic current after the addition of 1 mM Cs ions. These results indicated the need to understand the variation of anodic current as a function of the Cs ion concentration based on differential pulse voltammetry. The results as shown in Figure 3.5 (A) show the differential pulse voltammograms in the presence of varying concentrations of Cs ions.

The results as shown in Figure 3.5 (B) justify the dependence of the second redox couple of the PB nanoparticles on the cesium concentration; similar results revealed variation of the anodic current of the first redox couple of PB nanoparticles as a function of As(III) and

hydrogen peroxide concentrations. This observation indicated the dependence of the electrochemical behavior of PB nanoparticles on the nature of cations and suggested selectivity in the ion exchange electrochemical process. The results shown above indicate that the electrochemical response of the modified electrode was dependent on the analyte. Since cesium ions are associated with concentration-dependent electrochemical behavior that is analogous to that reported for cesium adsorption (Pandey et.al. 2021), the adsorption efficiency of the PB nanoparticle-modified SPE was considered.

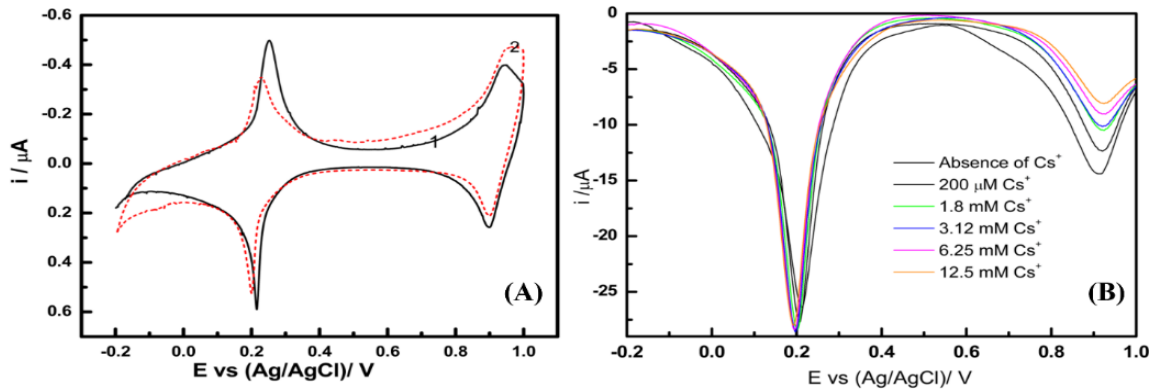

Figure 3.5. (A) Cyclic voltammogram of the PB nanoparticle-modified screen-printed electrode in 0.1 M KNO_3 at a scan rate of 10 mV/s in the absence (1) and the presence (2) of 1 mM Cs ions; (B) Differential pulse voltammetry of the PB nanoparticle-modified screen-printed electrode in the presence of varying concentrations of Cs ions.

3.2.2 Electrochemical Sensing of Cs ion through PBNP-modified Graphite Paste Electrode

3.2.2.1 Cyclic Voltammetry

Initially, we examined the sensing of cesium ions through the electrochemical behavior of Prussian blue-modified electrodes via cyclic voltammetry. Prussian blue displays two redox peaks; the first one is recorded at 0.2 V, which is attributed to Prussian white oxidation and Prussian blue reduction, and vice versa. In contrast, the second redox couple that appears at 0.9 V corresponds to Prussian blue oxidation to Berlin green reduction and vice versa. All cations promote Prussian blue. The only elements identified to be able to pass through the Prussian Blue lattice, aside from potassium, were ammonium (NH_4^+, cesium (Cs^+), and rubidium (Rb^+). Other divalent and monovalent cations are regarded as blocking ones. Prussian Blue undergoes complete oxidation at high anodic potentials because the equivalent set of peaks is present and the fully oxidized redox state is known as Berlin green. The only mechanism for charge compensation in Berlin Green/Prussian Blue redox activity is the trapping of anions throughout an oxidative reaction (Karyakin, 2001). Accordingly, we first examined the dependence of this redox-active reaction as a function of cesium ion concentrations. A typical cyclic voltammogram of PBNP-1/PBNP-2/PBNP-3 modified electrode in the presence and absence of 1 mM cesium ions is provided in Figure 3.6. The results demonstrate inconclusive findings on the dependence of the first redox peak as a function of the cesium ion concentration; however, some insight related to the dependence of the second redox couple on the cesium ion concentration was noted. Accordingly, we further attempted to record differential pulse voltammetry to obtain insight related to cesium ion sensing.

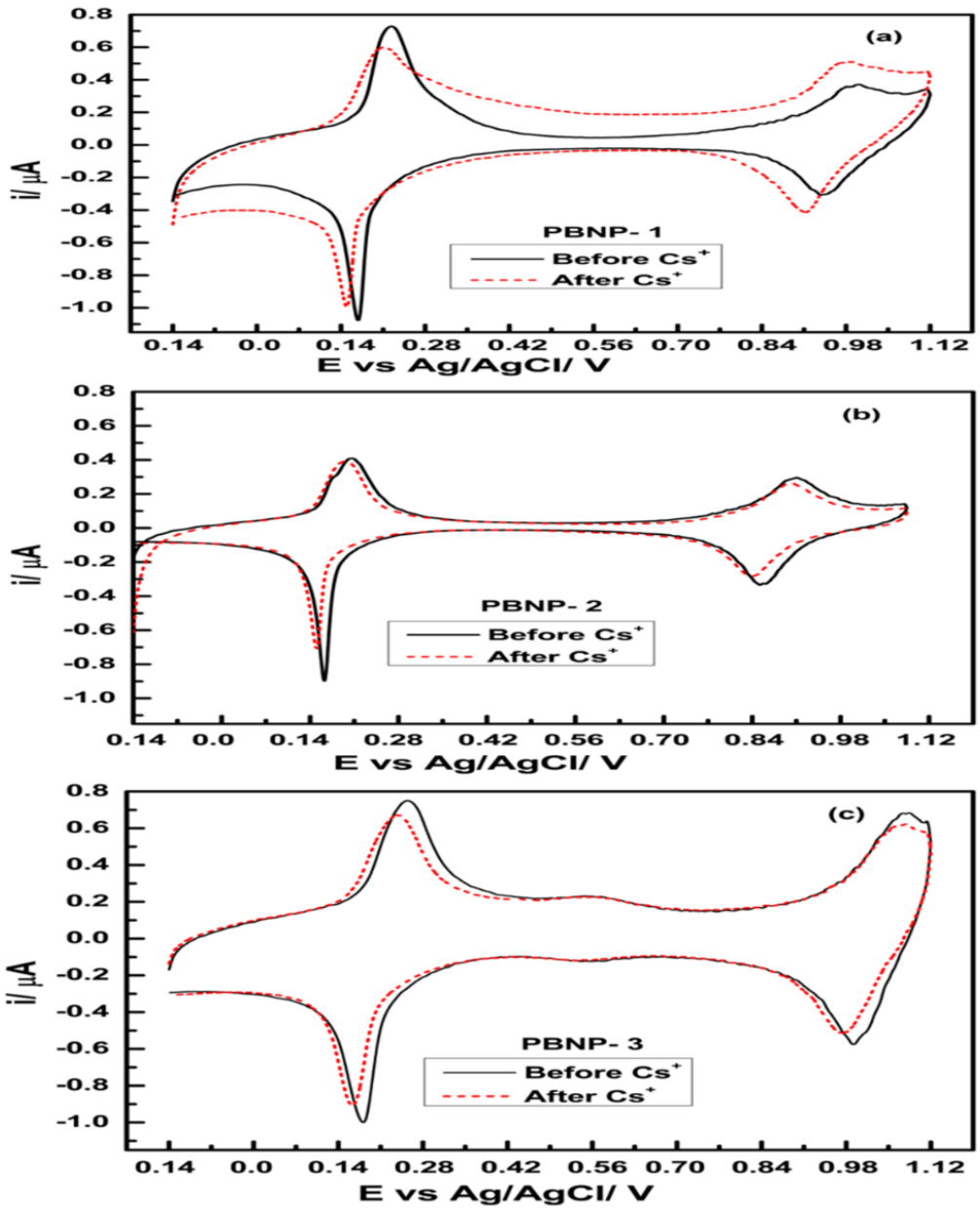

Figure 3.6. Cyclic voltammogram of (a) PBNP- 1, (b) PBNP- 2, and (c) PBNP- 3 at a scan rate of 0.01 Vs^{-1} in 0.1 M KNO3.

3.2.2.2 Differential Pulse Voltammetry

Electrochemical sensing of cesium ion with PBNP-1/PBNP-2/PBNP-3 modified electrode was evaluated from differential pulse voltammetry recorded between -0.2 to 1.0 V vs. Ag/AgCl as shown in Figure 3.7. Notably second redox couple of Prussian blue was found to be dependent on cesium ions; the peak current decreased with an increase in the cesium ion concentration. PB crystals have an intrinsic face-centered cubic structure with lattice spacing that is ideal for the hydration radius of Cs^+. The insertion of cesium ions into the PB lattice structure increases the tensile strength of the materials. Because of the chemical nature of cesium usually present in the form of salt that has relatively high solubility in water and to achieve cation adsorption PB is a very good candidate material. All three Prussian blue modified electrodes (PBNP-1/PBNP-2/PBNP-3) displayed similar behavior, with a sensitivity of about $8.5x10^{-4}$, $1.8x10^{-4}$, and $7.5x10^{-6}$, respectively. The different sensing functionality of the PBNP-1 was attributed to cationic polymer polyethyleneimine used as a spacer for Prussian blue nanoparticles. While PBNP-2 had THF-H_2O_2 and PBNP-3 contained EETMS as a spacer. EETMS can result in highly monodispersed nanosuspension responsible for better sensitivity (P.C. Pandey et al., 2021).

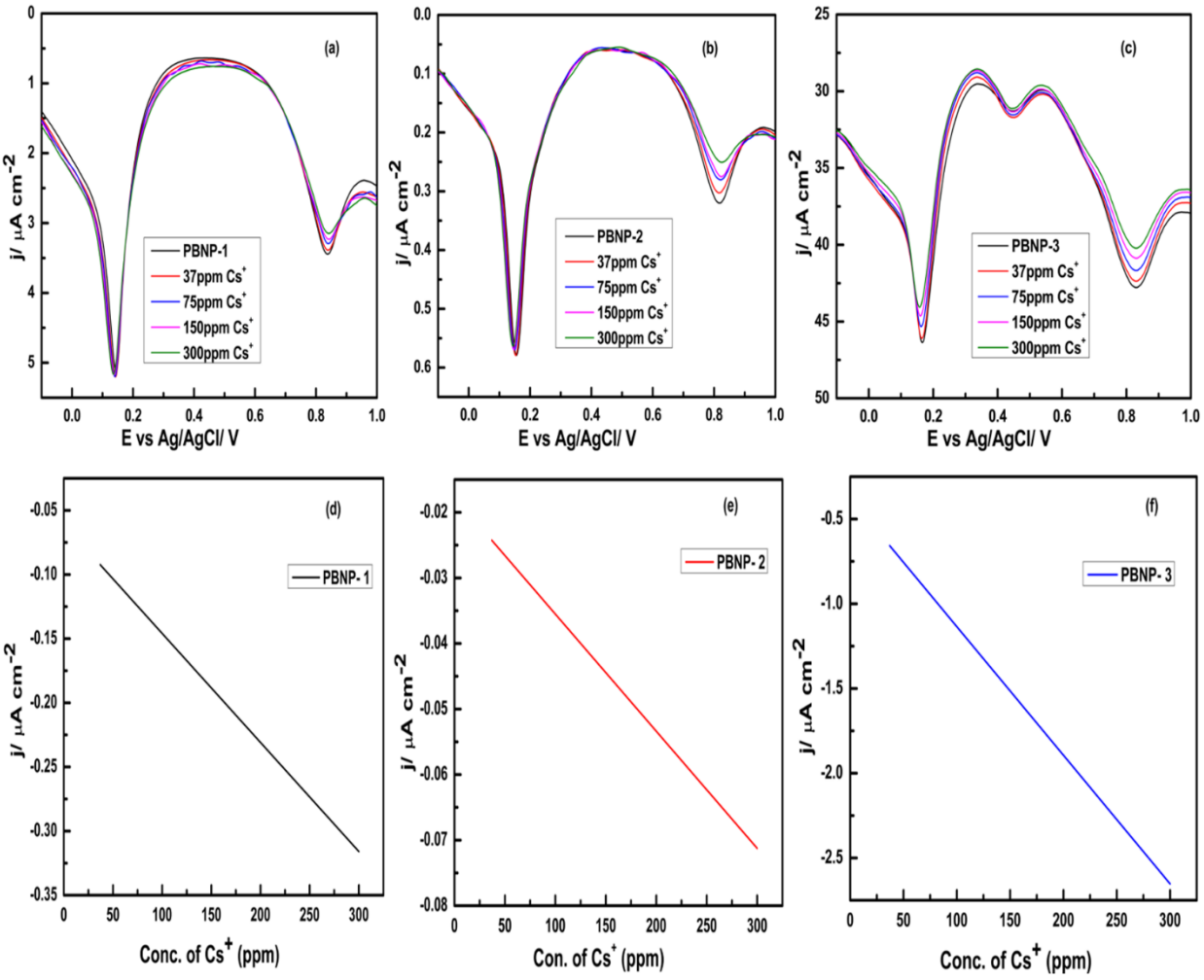

Figure 3.7. Study of Differential pulse voltammetry electrochemical response in the presence of Cs^+ (0-300 ppm) of (a) PBNP- 1, (b) PBNP- 2, (c) PBNP-3; concentration-dependent calibration curve of Cs^+ for (d) PBNP-1, (e) PBNP- 2, and (f) PBNP-3.

3.2.2.3 Electrochemical Impedance Spectroscopy

EIS was used to characterize the stepwise creation of the Prussian blue modified electrode in the absence and presence of cesium ions since it was an efficient technique for evaluating the

interference features of surface-limited electrodes. The impedance was measured with a CHI Electrochemical workstation between 1 Hz and 10 kHz at the appropriate polarization potential, which supported the cesium ion interaction as shown by cyclic voltammograms. In the absence and presence of cesium ions, a semicircle region of the Nyquist plot reflecting charge transfer resistance and a linear component representing a diffusion-limited process are present. The almost straight line that the bare PB nanoparticle-modified electrode presented in its EIS can be used to identify the diffusion-limiting stage of an electrochemical process. The semicircle's diameter corresponds to the electron-transfer resistance (Ret).

Figure 3.8 displays the electrochemical impedance spectroscopy results from the modified PBNP-1, PBNP-2, and PBNP-3 electrodes in the presence and absence of several concentrations of cesium ions. The semicircle section of the impedance spectra depicted in Figure 3.8 corresponds to charge transfer resistance; the linear section of the spectra corresponds to a diffusion-limited process. The nearly straight line indicated the diffusion-limiting step of the electrochemical process that the EIS of the bare Prussian blue nanoparticle-modified electrode (Figure 3.8) displayed. The diameter of the semicircle and the electron-transfer resistance (Ret) are related. In contrast to the Prussian blue nanoparticle-modified electrode in the presence of cesium ions, the semicircle diameter for the Prussian blue nanoparticle-modified electrode tended to increase.

The charge transfer resistance increased with an increase in the cesium ion concentrations as shown in Table 3.1; this result indicates that the predominantly diffusion-limiting step of the electrochemical process takes place between the Prussian blue nanoparticles and the Cs ions.

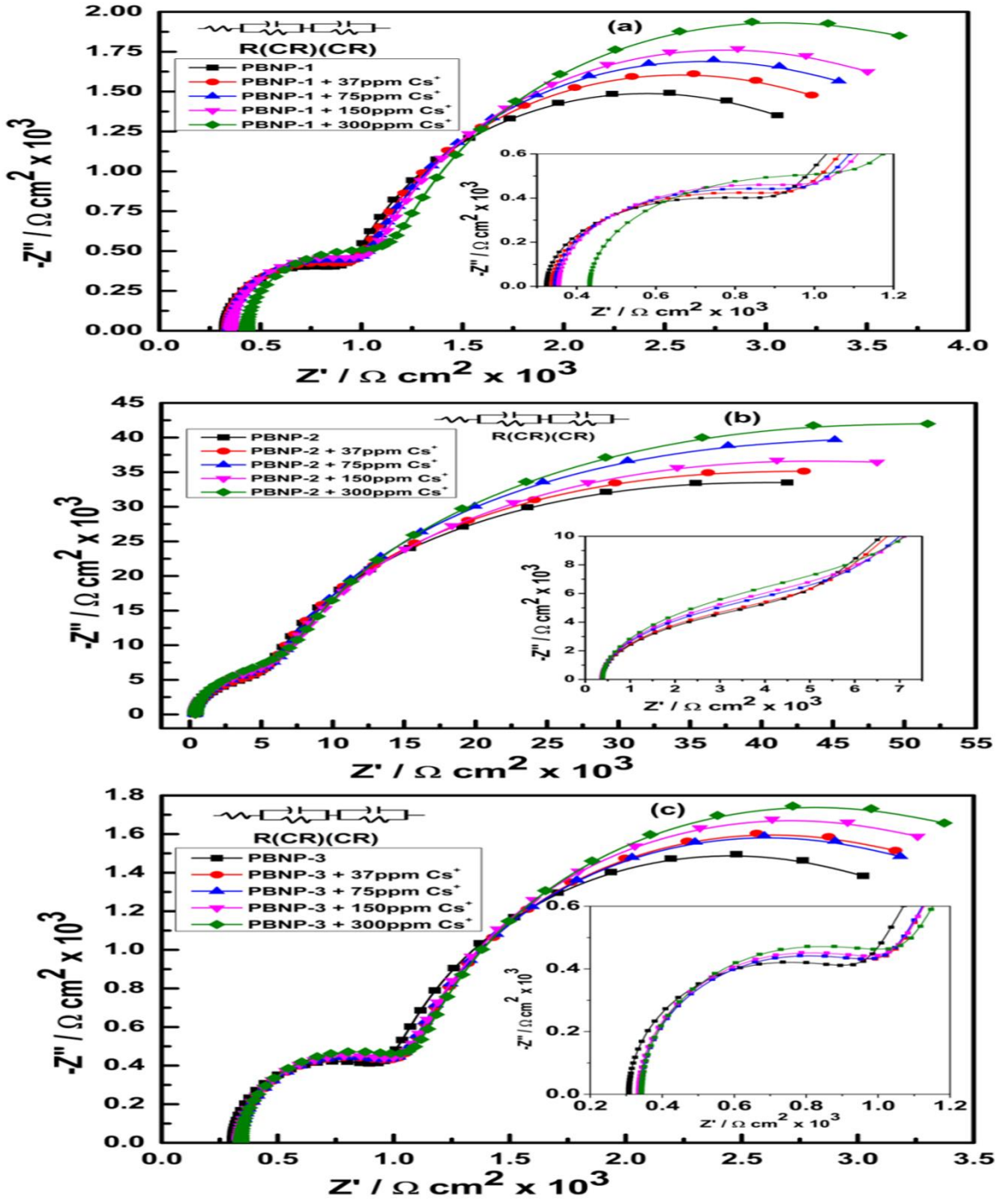

Figure 3.8. Nyquist plot of the (a) PBNP- 1, (b) PBNP-2, and (c) PBNP-3 modified electrode in the presence of varying concentrations of Cs^+ 406 (0-300 ppm).

Table-3.1. Dependence of Ret value of PBNPs on cesium ion concentration

Cs^+ conc. / PB	PBNP-1 R_{et}	PBNP-2 R_{et}	PBNP-3 R_{et}
Blank (without cs^+)	1.18×10^3	7×10^3	1.15×10^3
37 PPM	1.25×10^3	8×10^3	8×10^3
75 PPM	1.40×10^3	9×10^3	1.27×10^3
150 PPM	1.52×10^3	10×10^3	1.30×10^3
300 PPM	1.75×10^3	12×10^3	1.45×10^3

3.3 Sensing of cesium ions based on Magnetic Measurements

The name "Prussian blue" refers to polynuclear hexa-cyanometallates, which have a cubic crystal structure with a three-dimensional …. N-MIII-N-C-MII-C…. configuration and form a supramolecular network. If MII and MIII are paramagnetic transition metal ions, then they introduce magnetic properties such as ferromagnetism (Köhler et al., 2015). Accordingly, PBNPs may display superparamagnetic characteristics as a function of temperature. The synthesized PBNPs displayed super-paramagnetism with high saturation, zero coercivity, and remanence. Even at room temperature, the paramagnetic behavior is relatively low. Cesium ions residing in the cubic holes of the lattice may balance out the charge differences between MII and MIII, altering the paramagnetic properties. Accordingly, we investigated the change in the paramagnetic ability of PBNP as a function of cesium ion centration.

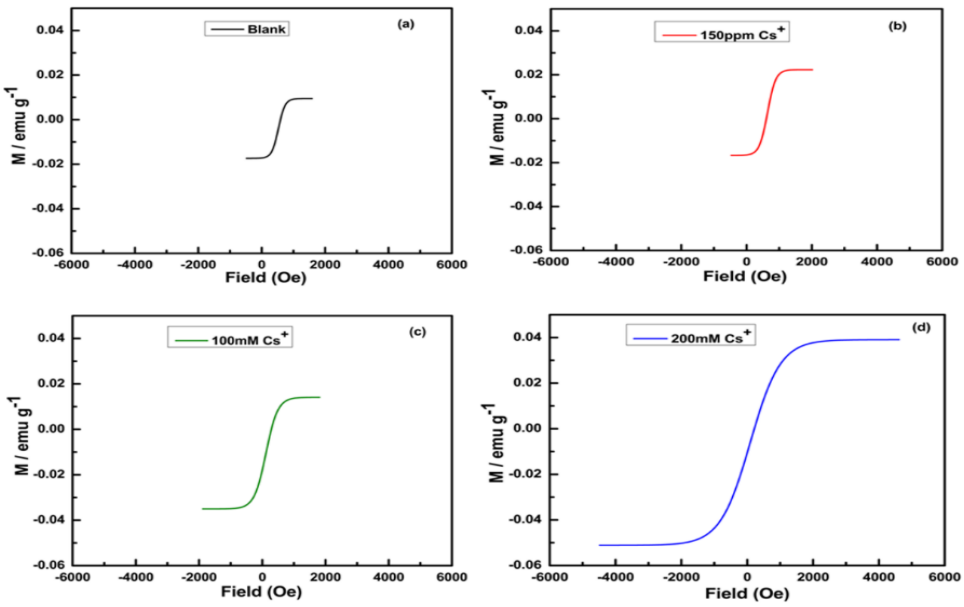

Figure 3.9. Magnetization hysteresis loops at 2K of PBNP-1 at different concentrations of Cs^+: (a) without Cs^+, (b) 150 ppm, (c) 100 mM, and (d) 200 mM.

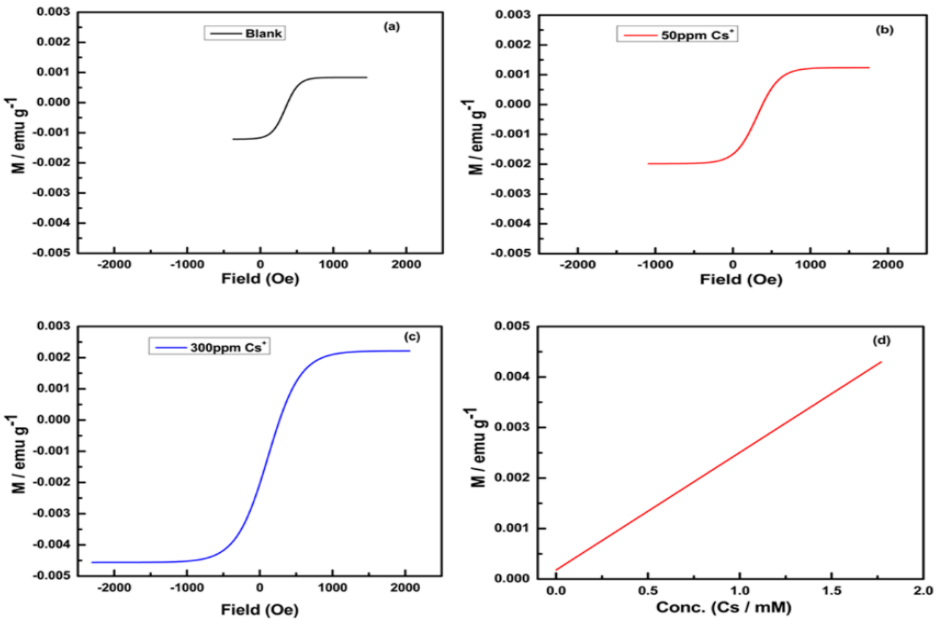

Figure 3.10. Magnetization hysteresis loops at 2K of PBNP- 2 @MSNP at different concentrations of Cs^+: (a) without Cs^+, (b) 50 ppm, (c) 300 ppm, and (d) calibration curve.

Notably, the paramagnetic functionality of PBNPs in both homogeneous and heterogeneous phase (within the mesoporous matrix) is altered dramatically in the cesium ions; this result provides excellent information on the sensing and removal of cesium ions based on PBNP formulation in homogeneous and heterogeneous phase. Figure 3.9 displays the variation in the magnetic property of PBNP powder as a function of cesium ion concentration, indicating the dependence of the paramagnetic character of PBNP on cesium ion concentration.

Further, PBNP-2 present in heterogeneous phases, especially within mesoporous silica nanoparticles, may serve as a potential adsorbent for cesium ion removal; accordingly, we investigated the ability of PBNP incorporated mesoporous silica for cesium ion sensing based on magnetic measurements. Cesium ions of variable concentrations of 10 to 600 ppm were incubated with PBNP-2 incorporated mesoporous silica, followed by resultant heterogeneous matrix collection, washing, and drying. The magnetic measurement of cesium-adsorbed PBNP-2 within mesoporous silica was examined as shown in Figure 3.10. The results clearly indicate that the magnetic properties of PBNPs vary as a function of cesium ion concentration. Nanoparticles of PB had a high adsorption surface area for cesium ions (Yang H. et al., 2014). The magnetic property thus can increase with Cs ions concentration due to its increased adsorption on PBNPs. Also, dipolar signal shifts arise through-space interactions between electron and nuclear magnetic moments, as well as through-bond transfer of spin to the Cs ions can result in a change in magnetic property. This could be attributed to cesium nucleus interaction with the unpaired electron localized at M^{II} or M^{III} and, at C and N atoms (Kohler F.H. et al., 2015). Therefore, the change in magnetism property of PBNPs gives an insight into the effective adsorbent behavior of PBNP-2 incorporated mesoporous silica in the removal of radioactive cesium from contaminated water.

3.4 Fluorometric Sensing of Cesium ions-based PBNP mediated Fluorescence Quenching of Fluorescein

The present study investigates the efficacy of Prussian blue nanoparticles as a quencher for the removal of cesium, utilizing fluorescence spectroscopy (Pandey et.al. 2021; Pandey et. al., 2020). Previous studies have shown that Prussian blue nanoparticles synthesized using 3-APTMS and cyclohexanone exhibit light-quenching properties (Pandey et.al. 2021; Pandey et. al., 2020). These nanoparticles have the potential to quench fluorescence radiation emitted within the visible range, thereby demonstrating their quenching ability. Prussian blue has a tendency to agglomerate over time, which renders the material photochemically inactive (Pandey et al. 2021; Pandey et al., 2020). However, the stability of Prussian blue in its nano shape is an essential prerequisite for fluorescence quenching. Accordingly, the Prussian blue nanoparticles, as reported herein in PBNP-1, PBNP-2, and PBNP-3, are used as a fluorescent quencher of standard fluorophore-fluorescein. Prussian blue refers to the formation of PBNPs from a single precursor, potassium ferricyanide, allowing an uncontrolled ratio of ferrous/ferric ions and hexacyanoferrate ions to yield a definite proportion of FeII-C-N-FeIII within the polymeric network and precisely allowing the interaction of cesium ions during the removal process. A Hitachi F-7000 fluorescence spectrophotometer measured the fluorescence. Since, Prussian blue nanoparticles act as a light quencher, the emission spectra of known luminescent/fluorescent materials are expected to be greatly quenched in the presence of Prussian blue nanoparticles. Fluorescein, a well-known fluorescent substance, is used for such measurements. Fluorescein aqueous solutions of known concentration (10^{-7} M) were utilized under various circumstances: The fluorescence spectra of (i) fluorescein alone, (ii) fluorescein and metal Prussian blue nanoparticles, and (iii) fluorescein, Prussian blue

nanoparticles, and varying concentration of cesium ions were recorded for cesium ion fluorescence sensing (Figure 3.12). The findings demonstrated that, in contrast to PBNP-2 and PBNP-3, PBNP-1 produced using the cationic polymer polyethyleneimine resulted in a Cesium ion concentration-dependent fluorescence response, which is primarily attributed to fluorescence energy transfer in the presence of cesium ions when the cationic polymer was used as a spacer for Prussian blue nanoparticles. In contrast, the other two do not show a significant change in cesium ion concentration-dependent fluorescence variation.

A fluorometric method was utilized to understand cesium-mediated fluorescence quenching; the obtained values were compared to those recorded for As(III) as reported earlier (Pandey et al., 2021). Fluorescein was used as a probe molecule (λex = 480 nm, λem= 510 nm). The fluorescence experiment was performed using neutral pH (6.8) with Milli-Q water. The optical properties of Prussian blue show a broad optical adsorption over 550 nm to 800 nm, corresponding to the blue region. It should be noted that fully oxidized PBNP thin films exhibit a lower absorption peak at 760 nm. However, the fully reduced state of the same as PW absorbs quite weakly in the visible region, resulting in a transparent state. The optical absorption coefficient value for a semiconductor may be represented by its direct/indirect optical band gap. The band gaps previously recorded by Qiu et al. for PB, PY, and PW have been described on the order of 1.75 eV, 2.02 eV, and 3.53 eV, respectively (Qiu et al., 2020); these parameters indicate that the optoelectronic properties of PB-related compounds should be controlled for cesium ion sensing. We have previously reported that PBNP acted as a fluorescence quencher (Pandey et al., 2021; Pandey et al., 2020). Accordingly, we investigated the fluorescence quenching ability of the well-known fluorophore fluorescein, which exhibits excitation and emission spectra at 494 and 521 nm,

respectively. Figure 3.11 shows the fluorescence quenching ability of PBNP-1, PBNP-2, and PBNP-3 on fluorescein emission Figure 3.11 (a-c). This finding clearly predicts excellent fluorescence quenching of Prussian blue nanoparticles with a quenching constant as calculated from the Stern-Volmer (S–V) plot (Mitra et al., 2022). The values of the quenching constant were found to be 10283 M^{-1} s^{-1}, 15737 M^{-1} s^{-1}, and 21181 M^{-1} s^{-1} for PBNP-1, PBNP-2, and PBNP-3, respectively, as indicated in Figure 3.11 (d); these results confirm the excellent quenching functionality of the as-made Prussian blue nanoparticles. PBNPs cause efficient quenching of fluorescein fluorescence; this phenomenon is likely due to the energy transfer process between fluorescein as donors and PBNPs as acceptors. In the stable functional PBNPs made using PEI/organotrialkoxysilane/THF+H2O2 as a reagent, the reagent protects the nano-geometry of PBNP for specific applications and behaves as a specific spacer to meet the requirement of energy transfer as discussed earlier (Pandey et al. 2021; Pandey et al., 2020). Accordingly, we further investigated the variation of the fluorescence quenching functionality of the as-made PBNPs in the presence of cesium ions. Notably, PBNP-2 and PBNP-3 showed very poor variation in the fluorescence quenching of fluorescein as a function of cesium ions; on the other hand, PBNP-1 displayed cesium ion concentration-dependent quenching functionality as shown in Figure 3.11. The quenching ability of PBNP-1 decreased with increasing cesium ion concentration. The reason behind this variation might be associated with the charge available around the spacer that may alter the quenching ability of PBNPs in the presence of charged cesium ions. The neutral spacer may not participate in altering the field quenching ability of PBNP; on the other hand, the charged spacer-like cationic polymer PEI may alter the quenching ability of PBNP. Since PBNP-1 is derived from a cationic polymer, Polyethyleneimine, an excellent result of the decrease in the

quenching ability of PBNP-1 is recorded as a function of cesium ion concentration (Figure 3.12a). A linear relation between cesium ion concentration and quenching extent in terms of percentage quenching of PBNP is recorded as shown in Figure 3.11 (d), justifying the innovative results from cesium ion sensing via fluorescence measurements.

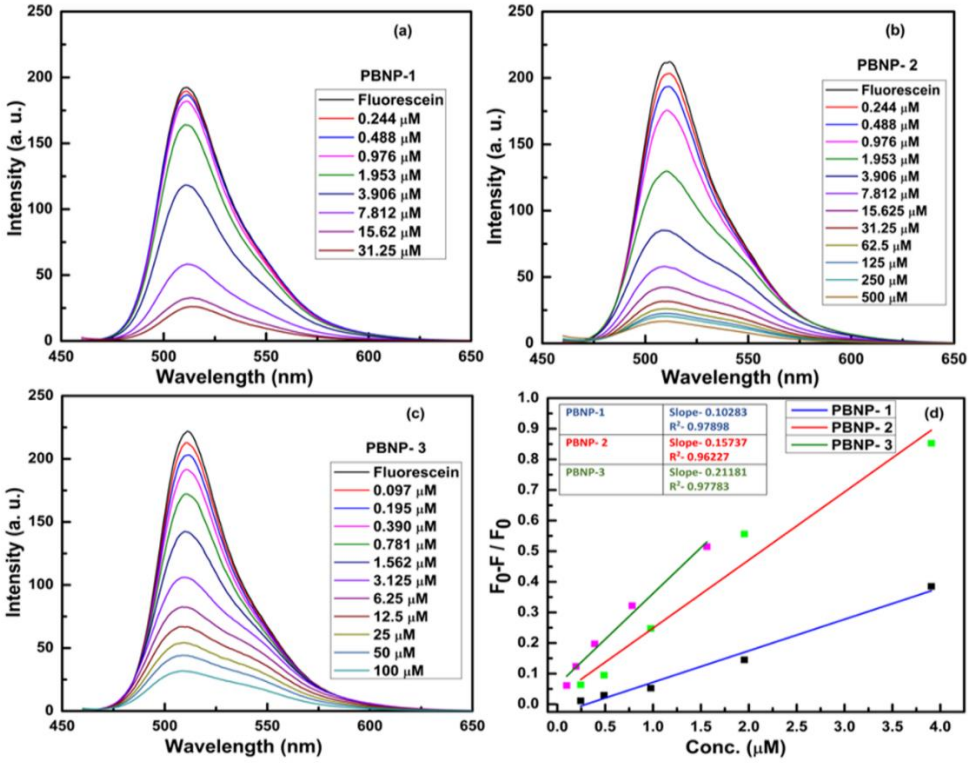

Figure 3.11. Dependence of fluorescence emission intensity on PBNP concentration between 0.1 and 500 mM for (a) 445 PBNP-1, (b) PBNP- 2, and (c) PBNP- 3; (d) Stern-Volmer (S-V) plot shows the kinetic parameter of PBNPs.

We further examined the difference in the quenching ability of PBNPs and $K_3[Fe(CN)_6]$, if any, to understand the impact of made PBNPs from the single precursor potassium ferricyanide (Figure 3.12 b). Figure 3.12b shows the results of this study, which indicate that $K_3[Fe(CN)_6]$ is not a

fluorescent quencher and confirms the requirement of both MII and MIII Fe ions for fluorescence quenching functionality.

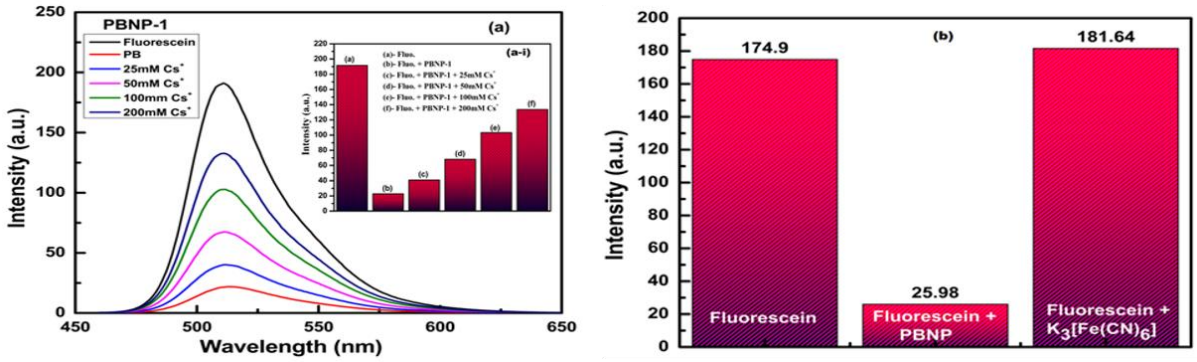

Figure 3.12. (a) Fluorescein in the absence and in the presence of different concentrations of Cs^+ (0-200 mM) and PBNP-1, (a-i inset) bar graph in the presence and absence of Cs^+ concentration with PBNP-1, and (b) fluorescein in the presence of PBNP and $K_3[Fe(CN)_6]$.

3.5 Measurement of ^{137}Cs radioactivity and determination of adsorption distribution coefficient (K_d) for cesium adsorption

The study assessed the cesium uptake efficacy of the material through a batch process involving the equilibration of 0.1 g of the sorbent and 10 mL of feed solution for 2 hours at room temperature, followed by an overnight standing period. A test solution containing 5g/L $NaNO_3$ spiked with ^{137}Cs radiotracer is used to determine the batch distribution coefficient for Cs. To better understand the ion exchange isotherm for Cs, test solutions with various Cs concentrations ranging from 1 to 1000 ppm were generated by dissolving the required quantity of $CsNO_3$ solution in 5 wt.% $NaNO_3$ solutions and then loaded with ^{137}Cs tracer. The kinetics of the adsorption was studied using a feed solution having 10 ppm Cs spiked with ^{137}Cs tracer. After equilibration, a 0.2-micron syringe filter

was used in each instance to filter the solution. The filtrate was analyzed for ^{137}Cs by counting using NaI/Tl scintillation detector coupled with a single-channel analyzer.

3.6 Assessment of Electrochemical Adsorption

The electrochemical adsorption (EA) was evaluated in 1 ppm Cs^+ solution at 0.25 V under stirring using chronoamperometry. For chemical adsorption (CA), procedures similar to the EA method without potential were undertaken. After adsorption, the Cs^+ ions in the solution were measured by ICP-MS. The Cs^+ removal performance was calculated using removal efficiency (R%) and uptake capacity (Q_e) values as follows (Rykov, A.I. et al., 2013; Zheng, Y. et al., 2017; Chen, R. et al., 2013):

$$R\% = \frac{(C_0 - C_e) \text{ x } 100}{C_0}$$

$$Q_e \text{ (mg/g)} = \frac{(C_0 - C_e) \text{ x V}}{\text{M}}$$

In this equation, Co and Ce are the initial concentrations of the cesium ions before adsorption and after adsorption at the equilibrium state, respectively, V is the volume of the solution, and M is the mass of the adsorbent.

The mechanism of electrochemical adsorption mode was identified following both single and multilayer adsorption curves using the Langmuir and Freundlich adsorption isotherm, respectively; the relevant equations are given below:

$$Q_e = \frac{Q_{max} \text{ x } K_L \text{ x } C_e}{1 + K_L C_e} \quad \text{for Langmuir adsorption isotherm}$$

$$Q_e = K_F C_e \, {}^{1}/_{n} \quad \text{for Freundlich adsorption isotherm}$$

In this equation, Q_{max} (mg g^{-1}) is the maximum adsorption capacity, K_F (L mg^{-1}) is Freundlich constant related to adsorption capacity, K_L (L mg^{-1}) is the Langmuir constant related to the free energy of adsorption, and n is the Freundlich exponent.

The selectivity for Cs^+ is determined from the distribution coefficient (K_d) using the expression below (Zheng, Y. et al., 2017):

$$K_d \text{ (mg/g)} = \frac{(C_0 - C_t) \text{ x V}}{C_0 \text{ x M}}$$

The K_d value was obtained using EA or CA system in the presence of 1 mM interfering alkali ions containing 1 ppm Cs^+ ions. The Cs^+ ions in the solution were monitored by ICP-MS.

3.7 Prussian blue nanoparticles inserted biocompatible mesoporous silica for removal of cesium ion from contaminated water based on inductively coupled plasma resonance spectroscopy

Prussian blue nanoparticles inserted mesoporous support (50 mg) were incubated overnight with different concentrations of cesium ions between 1 ppm to 50 ppm. After that, the cesium ion that had been adsorbed onto the PBNP-modified mesoporous support was centrifuged to separate it, and then ICP spectroscopy was used to check for the presence of cesium ion in the supernatant. The distribution coefficient, K_d value was calculated as 3.5×10^4 even at 3% PB content within the heterogeneous matrix. The 3% loading of PB nanoparticles in the composite corresponds to ~10.2 mmol of PB in the materials whereas the Cs ion present in the solution is in the pico-molar range.

Hence the active site available for exchange is very high compared to the Cs ion concentration present in solution. So, at this very dilute condition, the significantly higher K_d value indicates that most of the ion sites are available for Cs exchange and this is due to the nano-size effect of the composite. The PBNP-modified mesoporous support performed as a biocompatible adsorbent for cesium ion removal, demonstrating efficient biocompatible support for cesium removal from contaminated water.

3.8 Removal of Cesium ion

3.8.1 The Electrochemical Adsorption (EA) Performance of PB Nanoparticle-Modified SPE

The electrochemical adsorption (EA) of Cs^+ ions was evaluated by chronoamperometry using 1ppm Cs^+ solution. Chronoamperometric curves of the PB nanoparticle-modified SPE at various applied potentials in 1 ppm Cs^+ solutions were developed. The cathodic current fell at the initial stage, which reflected the creation of double-layer capacitance; it then approached the Cs^+ adsorption balance at a steady state. Figure 3.13 shows that Cs^+ adsorption showed optimum potential at 0.88 V; at this potential value, Cs^+ adsorption is driven by a large cathodic current. The use of the EA system for Cs^+ removal was evaluated using ICP-MS analysis; Q_e and R% data were obtained for the pure PB nanoparticle-modified SPE in 1 ppm Cs^+ solution with the EA system after 1h polarization at 0.88 V vs. Ag/AgCl. The removal performance of Cs^+ ion using the CA system was also investigated for the PB nanoparticle-modified SPE;

a larger Qe of 181 mg g^{-1} with 95% Cs^{+} ion removal was obtained using this EA system. The Q_{max} value of the PB nanoparticle-modified SPE for Cs^{+} ion was 325 mg g^{-1} when the Cs^{+} ion equilibrium concentration reached up to 50 µM; these adsorption data were in good agreement with the Langmuir isotherm. The K_d value for the PB nanoparticle-modified SPE reached up to 580 L g^{-1}, indicating efficient performance for cesium removal. Similar procedures are being adopted to make CuHCF-modified SPEs with enhanced performance for cesium removal as reported earlier (Zheng, Y. et al., 2017). A comparison of the adsorption parameters using various forms of adsorbents based on Prussian blue and its analogs is given in Table 3.2, which indicates the advantage of the PBNP-modified electrode in cesium adsorption.

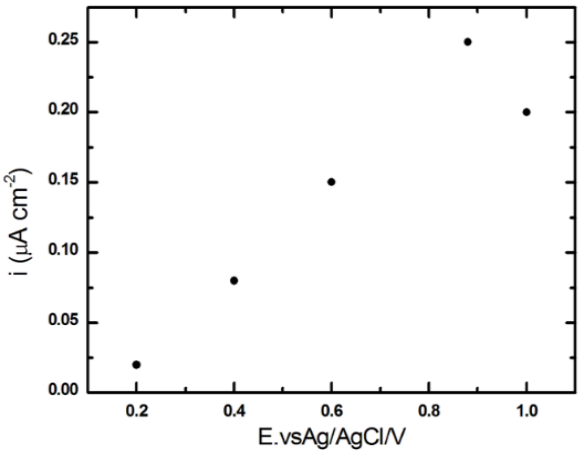

Figure 3.13. The dependence of chronoamperometric steady current response on the applied potentials.

Table 3.2: Prussian blue (FeHCF) and its analog-based adsorbents for cesium removal.

PB-Based Adsorbent	Removal Efficiency (%)	K_d L/g	Initial Conc. mg/L	Isotherm	Kinetic Model	Q_{max} mg/g	Reference
MWCNT–CuHCF	95	568	1	Langmuir Freundlich	NA	310	Zheng, Y. et al., 2017
SWCNT–CuHCF	NA	NA	NA	NA	NA	230	Draouil, H. et al., 2014
MWCNT–Na–CoHCF– alginate	53	23	200	Langmuir Freundlich	PFO PSO	133	Vipin, A.K. et al., 2014
Fe_3O_4–FeHCF–GO–alginate beads	80	48.7	25-150	Langmuir Freundlich	PSO	43.5	Yang, H. et al., 2014
Fe_3O_4–FeHCF–hydrogel	99.5	0.4	100-400	Langmuir	PSO	41.5	Yang, H. M. et al., 2018
Chitosan–FeHCF–CNT	NA	42.5	1-100	Langmuir Freundlich Redlich Peterson	PFO PSO	219	Li, T. et al., 2016
rGO–FeHCF	99.5	6.46	0.2	Langmuir Freundlich	NA	18.67	Jang, S.C. et al., 2015
FeHCF-modified screen-printed electrode	95	580	1	Langmuir Freundlich	NA	325	**Present work**

3.8.2 ^{137}Cesium ion removal through PBNP-2 incorporated mesoporous silica

One of the major tasks of the current study is to evaluate the materials for use as an efficient biocompatible matrix for ^{137}Cs removal from contaminated water. Adsorption is a cost-effective approach to remove cesium ions from contaminated water. The transport of cesium from contaminated water to the surface of a solid matrix is implied by this separation process (i.e., PBNP-2 incorporated mesoporous silica as an adsorbent).

A material for this application should possess a tailored surface chemistry and porosity to obtain effective cesium ion separation (as evident from Figure 2.3); this approach justifies the synthetic incorporation of PBNPs within mesoporous silica. The results recorded in Figure 2.2 (previous chapter) on XRD and PBNP-2 incorporated mesoporous silica and the BET results shown in Figure 2.9 (previous chapter); confirm the formation of PBNP-2 incorporated mesoporous silica matrix as a potential ^{137}Cs ion adsorbent. After the magnetic measurements were obtained, we examined the binding ability of PBNP-incorporated mesoporous silica-based using energy-dispersive X-ray analysis. Figure 3.14 shows the findings from the adsorption of cesium ions at different concentrations that were present in contaminated water (Table 3.3). Data were obtained in the absence of cesium ions (Figure 3.14 A) and the presence of 300-ppm cesium ions (Figure 3.14 B). Figure 3.14 clearly confirms the efficient binding ability of PBNP incorporated mesoporous silica for cesium ion removal. These findings were further confirmed by the measurement of cesium ions in the supernatant of these four samples by ICPE. The results clearly confirmed the efficiency of PBNP-2 incorporated mesoporous silica, which was noted to be highly suitable for the removal of cesium ions.

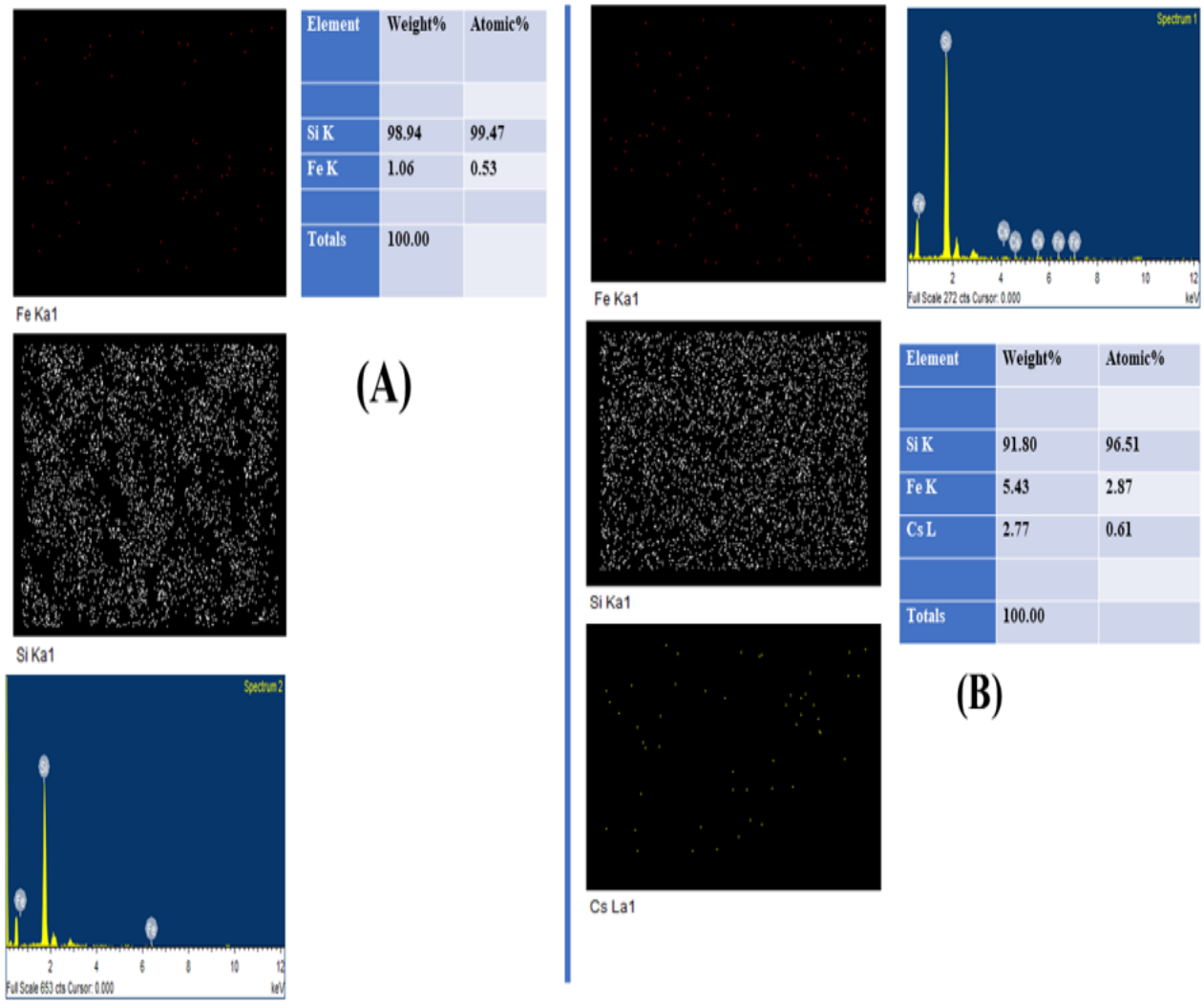

Figure 3.14. Mapping analysis of PBNP incorporated mesoporous silica in the absence of Cs^+; (B) Mapping analysis of PBNP incorporated mesoporous silica in the presence of Cs^+.

Table 3.3: ^{137}Cs uptake performance of PBNP encapsulated mesoporous silica (10% PBNP w/w within MSNP).

Sample	Wt. of the sample (g)	Vol. of Feed (mL)	V/M	Initial pH	Equi^{m}. pH	K_d
10% PBNP w/w within MSNP	0.100	10	100.00	7.25	4.99	31000 ±1500

We have further examined the functionality of PBNP-incorporated mesoporous silica for the removal of cesium ions based on the measurement of the radioactivity of ^{137}Cs ions. The adsorption coefficient of PBNP incorporated mesoporous silica based on the radioactivity measurement of ^{137}Cs was calculated as $3.5x10^4$ even at 3% Prussian blue content within the heterogeneous matrix, justifying the efficiency of the material for radioactive cesium removal as shown in Table 3.3. Figure 3.15 (a) shows the cesium adsorption isotherm of PBNP-incorporated mesoporous silica over an equilibrium Cs concentration range of 1 to 1000 ppm. Almost all of the Cs were taken up by the material at lower cesium concentration, followed by a sharp increase beyond 0.001 M Cs, indicating occupancy of all of the sites by Cs. Flattening of the curve beyond 0.001 M Cs signifies that attainment of equilibrium Cs uptake capacity. The maximum Cs sorption capacity (qe mmol/g) of the sorbent was calculated and found to be 0.1 meq/g, which is in good agreement with previously reported values as compared in Table 3.4. The adsorption isotherm described above was fitted using both Freundlich and Langmuir adsorption isotherm models are shown in Figure 3.15 (b) and Figure 3.15 (c).

The fitting parameters were obtained to give a mechanistic understanding of the surface properties and affinity of the sorbent. The Freundlich and Langmuir isotherm model equation can be represented as follows:

In the Freundlich model: $\ln q_e = \ln K_F + \frac{1}{\mathrm{n}} \ln C_e$ ..... (1)

K_F denotes the sorption capacity when the metal ion equilibrium concentration is equal to 1, and 1/n denotes the degree of sorption dependency with the equilibrium concentration.

In the Langmuir model: $\frac{1}{q_e} = \frac{1}{q_m} + \frac{1}{K_L C_e q_m}$ ..... (2)

In this equation, q_m and K_L are the maximum monolayer capacity and sorption coefficient, respectively.

As per fitting with the Freundlich model, the adsorption data shows a linear relationship (R^2=0.98); the values of K_F and 'n' as obtained from the log-log plot were found to be 5.23 and 1.34, respectively. This 'n' value indicates a monolayer adsorption of Cs taking place on the sorbent surface. Similarly, the fitting with the Langmuir model (R^2=0.99) culminated in q_e and K_L values of 0.037 mmol/g and 2280, respectively.

A study on the kinetics of adsorption is important towards having optimized uptake performance. Hence, the sorbent was contacted with a 10 ppm Cs solution for different time intervals; the uptake capacity of the sorbent as a function of time was shown in Figure 3.15 (d). It can be inferred that equilibrium is attained within 20 minutes with maximum uptake capacity.

Table 3.4. A comparison of previously reported LOD and maximum removal capacity of Cs^+ from water using PB.

Materials	Size	LOD	Maximum Removal capacity	References
PB embedded cellulose Nanofiber	1-2 µm	1 mg/L^{-1}	54.2 mg g^{-1}	Park et. al., 2023 (a)
Mn-Fe PBA	NA	0.013 mM	NA	Zhou et.al., 2021
Prussian Blue graphene hydrogel	NA	NA	4.67 mmol/g	Seema et.al., 2023
MBC-PB	NA	NA	52.3 mg/g	Park et. al., 2023 (b)
PAN-D-PB	NA	NA	186 mg/g	Gwon et. al., 2020
Prussian Blue	NA	NA	500 ppb Cs^+	Ohara et.al., 2021
Magnetic Prussian Blue/Reduced Graphene Oxide	NA	NA	3.64 mmol/g	Seema et al., 2020
PB@Fe_3O_4 microparticles	NA	NA	16.13 mg/g	Wang et. al., 2020
PBNP-2 incorporated mesoporous silica support	59 nm/ 200 nm	1.37 µM	0.1 mmol/g (13.29 mg/g)	**This Work**

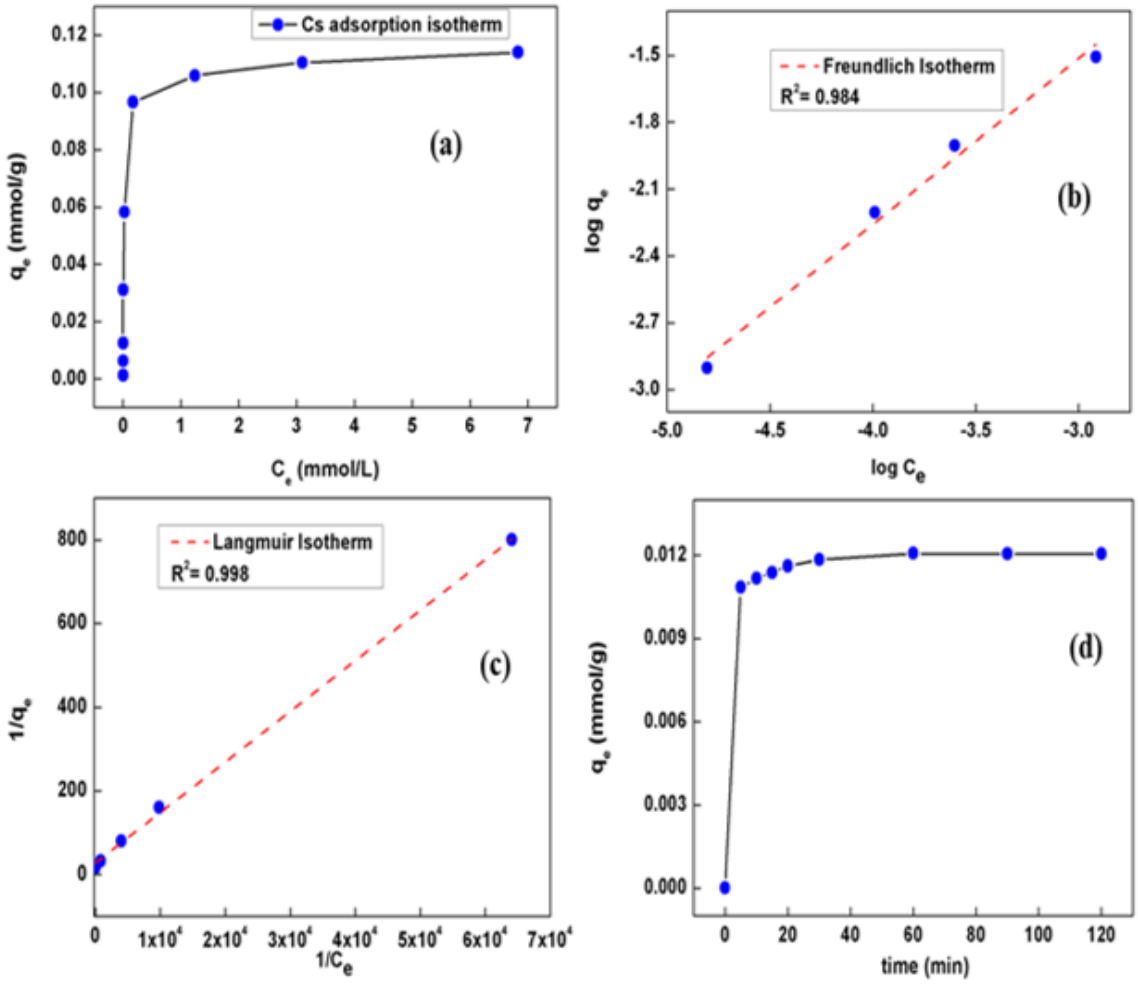

Figure 3.15. Cs^+ adsorption isotherm using (a) PBNP-2 incorporated mesoporous silica, (b) fitting of Cs^+ adsorption using Freundlich model, (c) fitting of Cs^+ adsorption using Langmuir model, and (d) kinetics of cesium uptake using PBNP incorporated silica.